Biophysical Chemistry 152 (2010) 55–64

Contents lists available at ScienceDirect

Biophysical Chemistry

journal homepage: http://www.elsevier.com/locate/biophyschem

Assessing protein–surface interactions with a series of multi-labeled BSA using fluorescence lifetime microscopy and Förster Energy Resonance Transfer

Denisio M. Togashi *, Alan G. Ryder

Nanoscale Biophotonics Laboratory, School of Chemistry, National University of Ireland, Galway, Galway, Ireland

ARTICLE INFO

Article history:
Received 15 June 2010
Received in revised form 13 July 2010
Accepted 28 July 2010
Available online 3 August 2010

Keywords:
Protein adsorption
Biomaterials
Fluorescence lifetime imaging
FRET
Confocal microscopy
Frequency domain
Bovine serum albumin

ABSTRACT

Reliably measuring the physicochemical properties of protein thin layers deposited on surfaces is critical to understanding the surface chemistry, biocompatibility, and performance of implanted biomaterials. Here we apply a series of multi-fluorophore labeled Bovine Serum Albumin (BSA) proteins as model probes to investigate surface-induced conformational changes of BSA by the use of a confocal Fluorescence Lifetime Imaging Microscopy and Förster Resonance Energy Transfer (FLIM–FRET) method. In this FLIM–FRET approach we study six different constructs where the BSA is covalently linked to one (BSA-F1) or five (BSA-F5) fluorescein molecules, one (BSA-T1) or seven (BSA-T7) rhodamine molecules, and hetero labeled with both (BSA-F4-T2 and BSA-F6-T1). The fluorescence intensity and decays were simultaneously measured at two different emission regions (green and red channels) of the labeled BSA deposited on substrates of different hydrophilicity and hydrophobicity. To generate reliable data, several different regions (10^4 μm^2 in each case) of the surfaces were scanned for each measurement. The amplitude-weighted lifetimes, obtained from the fluorescence decay parameters, are discussed based on the average distance between the conjugated fluorophores acting as a donor and acceptor pair in the Energy Transfer framework. The number of probes conjugated has significant effects on the fluorescence emission intensity and lifetimes in solution and on surfaces. The BSA-F4-T2 constructs showed a significant ability to differentiate using lifetime the hydrophilicity and hydrophobicity of the surfaces, by detecting local expansion and contraction of protein structure in the deposited layers. Using these multiple labeled BSA probes in conjunction with FLIM–FRET can provide a way to assess structural changes in proteins induced by variations in surface chemistry of biomaterials.

1. Introduction

Medical devices implanted in the human body are exposed to biological fluids which contain a wide variety of proteins that promptly deposit on their surfaces [1]. It is during the course of this process that the body may initiate a series of cascade reactions resulting in an inflammatory response [2]. Currently accepted thinking, suggests that the surface chemistry of the implant device can induce some structural changes in the adsorbed protein molecules, which can indirectly induce adverse reactions in the body [3]. In some cases after surgical implantation of a medical device (particularly cardiac stents) one must administer thrombolytic drugs [4] to avoid such adverse reactions. Another less invasive approach is to use drug-eluting coatings containing thrombolytic or antithrombotic drugs on the implant devices that minimize or prevent the inflammatory response [5,6].

The adsorbed protein layer which comes into contact with the biological environment is crucial to medical device biocompatibility. Understanding how surface materials interact with the adsorbed proteins can then first enable control of protein selectivity or adsorption rate, and second provide information on how to regulate the protein structural changes in the deposited layer [7]. Thus understanding in detail this complex protein–surface interaction will help in the design of smart and efficacious biomaterials. However, observing the structural changes in proteins during the adsorption process is a fundamentally difficult task, and many of the elementary processes involved in the protein–surface interaction still remain unknown, or are not capable of being observed in dynamic environments [8–10]. There are a wide variety of experimental approaches that can be applied to study protein–surface interactions, such as: depletion, radiotracer, quartz crystal microbalance, ellipsometry, total internal reflection fluorescence, neutron reflection, surface Plasmon resonance, atomic force microscopy, and time resolved evanescent wave-induced fluorescence anisotropy spectroscopy [11–16]. To gain a comprehensive understanding of the complex

* Corresponding author. Nanoscale Biophotonics Laboratory, School of Chemistry, National University of Ireland-Galway, Galway, Co. Galway, Ireland. Tel.: +353 91 49 5186; fax: +353 91 52 5700.
E-mail address: denisio.togashi@nuigalway.ie (D.M. Togashi).

0301-4622/$ – see front matter © 2010 Elsevier B.V. All rights reserved.
doi:10.1016/j.bpc.2010.07.006

protein–surface interaction, one needs to observe these interactions under dynamic conditions and thus one requires a suite of techniques, to study the different facets of the process [17].

Recently we demonstrated the use of Confocal Fluorescence Microscopy (CFM) in the quantification of protein deposited on hydrophilic glass [18]. Despite a rather complicated experimental procedure, and various limitations of the fluorescent label used, this proof of concept study demonstrated that the CFM method provides information on a variety of adsorption parameters. Any significant improvements in the basic CFM methodology, which is based on fluorescence intensity measurements, would require the use of a fluorophore whose emission properties are not affected by either the presence of amino acid quenchers or changes in protein structure (a rather unlikely scenario) [19]. Unfortunately, analytical methods based on fluorescence intensity measurements are fraught with inherent difficulties with regard to accurate intensity measurements (source and detector instabilities for example). A rational alternative is to utilize fluorescence lifetime based methods which offer an inherently more robust measurement method [20].

The fluorescence lifetime is the reciprocal of the sum of all transition rates from the excited fluorophore to the ground state. Fluorescence lifetime measurements are often used in preference to intensity based measurements because they can eliminate or minimize problems such as auto-fluorescence, source and detector instabilities or spectral shift. Lifetime measurements are also sensitive to the physicochemical parameters of the medium surrounding the fluorophore (pH, ion concentration, polarity, and so forth) and this can be used to extract useful information from complex environments [21]. For studying complex environments at sub-micron spatial resolution, confocal fluorescence lifetime imaging microscopy (FLIM) is rapidly becoming a widely applicable technique, more compact and user friendly [22–25]. The FLIM technique is normally used in the life sciences to create and/or improve image contrast, based on the fluorescence lifetime differences. Here, however, we applied FLIM specifically to obtain the fluorescence lifetime from samples (protein layers) in 2D. We were not interested in obtaining high spatial resolution images because of two factors: one, we need to avoid or reduce photobleaching effects, and two, even the best axial and/or lateral optical resolution does not allow one to observe only the deposited protein layer. We have demonstrated previously how FLIM can be used to study changes of protein conformation in adsorbed layers on different surfaces, where the measurement methodology involved the direct lifetime measurement of 1-anilino-8-naphthalene sulfonate (ANS) labeled Bovine Serum Albumin (BSA) [26]. This direct measurement was based on correlating changes in ANS lifetime due to the variations in ANS accessibility to the aqueous environment, with protein structural changes on adsorption [27].

In FRET where there is a good overlap between the absorption spectrum of the acceptor and the emission spectrum of the donor, with a relatively high fluorescence quantum yield, and the donor and acceptor dipoles are in an acceptable orientation, then the distance between the donor–acceptor pair can be calculated from the emission data (lifetime or intensity) of the donor. This allows for the observation of structural changes on the Angstrom scale. The use of lifetime (FLIM–FRET) instead of conventional intensity based FRET has numerous experimental advantages and the method has been used to analyze protein–protein interactions and structural changes [21,28,29]. Here we present our preliminary results in the development of a FLIM–FRET based protocol used to observe the interaction of proteins with hydrophilic and hydrophobic surfaces. The approach also involves the use of the well studied and readily available BSA, labeled with fluorescein (F) and Tetramethylrhodamine (TMR) fluorophores (a common FRET pair) as a model protein (BSA-F–T) for studying protein–surface interactions. The effect of different probe–protein molar ratios was also analyzed. Although, the presence of more than one conjugated probe could disturb the native structure of the protein, we are interested in the relative structural changes between the free solution and the adsorbed protein on a surface. This small alteration of the native structure can be ignored. When the labeled BSA adsorbs onto the different surfaces, the comparative measurements of the fluorescence lifetimes in the bulk and in the adsorbed layer provides information on FRET efficiency from which one can estimate the degree of structural change that the conjugated protein underwent from the bulk solution to the adsorbed layer medium.

2. Experimental methods

2.1. Materials

Fluorescein and Tetramethylrhodamine isothiocyanate labeled Bovine Serum Albumin proteins (BSA-F5 and BSA-T7 with molar ratios of 5 and 7, respectively, data provided by the suppliers) and 8-Hydroxypyrene-1,3,6-Trisulfonic Acid (HPTS) were obtained from Invitrogen. Bovine serum albumin (BSA) of purity 99%+ (catalog no. A7638), Tetramethylrhodamine isothiocyanate labeled Bovine Serum Albumin protein (BSA-T1), eosin, fluorescein isothiocyanate (FITC), Tetramethylrhodamine isothiocyanate (TMR), Rhodamine B (RhB), phosphate buffered saline tablets for 0.01 M phosphate buffer with 0.0027 M potassium chloride, and 0.137 M sodium chloride for pH 7.4 (PBS), Secure-Seal™ imaging spacers (0.12 mm thick with diameters of 20 mm and 9 mm) and CoverWell imaging chambers (1.0 mm thick with diameters of 20 mm and 9 mm), Sephadex G25, Whatman 25 mm GD/X 0.2 μm pore size, Ludox, RBS 35 detergent, were all obtained from Sigma-Aldrich. Common chemicals like dimethyl-dichlorosilane, trichloroethylene, methanol (spectroscopic grade), hydrogen peroxide (30%), nitric acid (69%), sodium hydrogen carbonate, dimethyl sulfoxide (DMSO) and sulphuric acid (98%) were obtained from either Sigma-Aldrich, Fisher Scientific, or AnalaR (sodium carbonate). All reagents were used without further purification; and solutions were made up with 18 MΩ resistivity deionized water (DIW) from a Milli-Q Millipore system.

2.2. Sample preparation

Glass substrates (microscopy cover glass N#1.5 and slide glass, from Menzel-Gläser or VWR International) with a hydrophilic surface were prepared as follows: a) substrates were first sonicated for 30 min in a solution of alkaline detergent, RBS 35, b) then soaked for 3 h in piranha solution (3:7) v/v H_2O_2:H_2SO_4, c) sonicated for 1 h in deionized water (DIW), d) rinsed with plenty of DIW and then stored in fresh DIW. The hydrophilic surfaces were converted to hydrophobic surface substrates with the following additional steps: e) dried overnight in air at 80 °C, f) then soaked in a solution of dimethyl-dichlorosilane (2%)/trichloroethylene, g) rinsed with trichloroethylene, methanol, and DIW, and h) stored in methanol solution at room temperature. The hydrophobicity and hydrophilicity were qualitatively assessed using water contact angles measured using the Bartell and Zuidema method and a digital camera [30]. The contact angles were approximately 16 ± 1 ($n = 4$) and 93 ± 1 ($n = 6$) degrees for the hydrophilic and hydrophobic surfaces, respectively. For protein labeling, a standard protocol was used as a reference [31]: 2–3 mg of protein (unlabelled or previously labeled) was dissolved in 1 ml of 0.1 M sodium carbonate solution. To prepare the singly labeled BSA-F1, and BSA-T2 constructs, protein:dye molar ratios of approximately 1:2 (BSA:FITC), 1:6 (BSA:TMR) were used. A small aliquot of 1.0 mM or 10 mM stock solution of FITC (or TMR) in DMSO was added to the unlabelled protein solution. To prepare the doubly labeled BSA-F6-T1, and BSA-F4-T2 constructs, a protein–fluorophore molar ratio of approximately 1:10 (BSA-T1:FITC and BSA-T2:FITC) was used. In the case of BSA-F6-T1 preparation, 3.2 mg of BSA-T1 was dissolved in 1 ml of 1 M sodium hydrogen

carbonate solution (pH 8.0) and then a small aliquot of stock of FITC was added. To prepare BSA-F4-T2 construct, 0.5 ml of the BSA-T2 solution, and 0.5 ml of 0.2 M sodium carbonate solution (pH 10.4) were mixed with the corresponding amount of FITC in DMSO. All the reactions were left for at least 3 h stirring in the dark at room temperature. Then a Sephadex filter was used to separate the labeled protein from the reaction mixture. The labeling degree or fluorophore per protein ratio (r) is calculated by [32]:

$$r = \frac{A_{494}}{A_{280} - A_{494} \times 0.3} \times \frac{\varepsilon_{280}}{\varepsilon_{494}} \quad (1)$$

0.3 is a correction factor to compensate for fluorophore absorption at 280 nm. A_{280} and A_{494} are the absorbance values at 280 nm and 494 nm. While ε_{280} and ε_{494} the molar absorption coefficients for protein and FITC at 280 nm and 494 nm, are 43,600 M^{-1} cm^{-1} and 68,000 M^{-1} cm^{-1} respectively [32,33]. In the case of TMR, A_{494} and ε_{494} are substituted, respectively, with the absorbance of the dye (A_{555}) and molar absorption coefficient ($\varepsilon_{555} = 65{,}000\ M^{-1}\ cm^{-1}$ [34]) at 555 nm in Eq. (1). In the BSA-F1 single label construct, the molar ratio between protein and fluorophore (BSA:FITC) ratio was around 1.18, while for labeling with TMR (BSA-T2), the ratio was approximately 1.8. For calculating the concentration of the doubly labeled protein, we assume that concentration can be determined from the optical absorption of the TMR center (A_{555}). Using this data, the FITC:TMR ratio of FITC on BSA-T1 and BSA-T2 can be calculated by:

$$r = \frac{A_{494} - 0.19 \times A_{555}}{\varepsilon_{494}} \times \frac{\varepsilon_{555}}{A_{555}} \quad (2)$$

0.19 is a correction factor to compensate for TMR absorption at 494 nm, A and ε are the absorbance and molar absorption coefficients values for the fluorescein (494) and rhodamine (555) centers. In the doubly labeled constructs, the FITC:TMR ratio was 2.2 and 6.1. This means that approximately 4 and 6 fluorescein molecules were covalently attached to the purchased BSA-T2 and BSA-T1, generating the BSA-F4-T2 and BSA-F6-T1 constructs respectively.

To study the protein–surface interaction, two sample protocols were followed. Both involved incubating the surface with the labeled protein solution, but in one case the labeled solution was removed after the incubation period and replaced with buffer prior to measurement (PS−). In the other case, the lifetime measurements were made with the original labeled protein solution in place above the surface (PS+). The sample chambers used for the measurements were made by sticking an imaging spacer to the surface of the hydrophilic or hydrophobic surface material (made from glass microscope slide or cover slip) and then sealing after addition of the solution with the hydrophilic or hydrophobic glass microscope cover slip (Fig. S1, Supplementary data). The PS+ samples were prepared by filling the chambers with the various labeled proteins in PBS buffered solution, with concentrations below 3 μM. The chambers were then sealed and the system was equilibrated for at least 4 h at room temperature before making any measurements. A near identical protocol is used for the preparation of the PS− samples, except that the chamber is kept open during the incubation period. To avoid evaporation of the protein solution, the imaging spacer chamber was left in a water saturated atmosphere (for more details see Supplemental data, Fig. S2). After, the required incubation period, the bulk labeled protein solution was removed with a pipette, the sample well rinsed at least 3 times with PBS buffer, then a fresh aliquot of PBS buffer solution was placed in the chamber before finally closing the chamber with a microscope cover or glass slide. For the PS− samples, measurements were made where the fluorescence signal is observed at the substrate interface; no significant fluorescence detection was observed in the bulk region above the interface during the experiments.

2.3. Instrumentation

UV–visible absorption spectra were recorded using Shimadzu UV-1601 or Lambda 950 Perkin Elmer spectrophotometers. Steady-state fluorescence measurements in 2 mm path length cuvette cells at room temperature were made with Perkin Elmer LB50B or Cary Eclipse spectrofluorimeters. FLIM measurements were made using an Alba system (ISS, Champaign, Illinois) based on an upright Olympus BX51 microscope (Fig. 1). The lifetime measurements are made using the phase-modulation method with frequencies in the 1–300 MHz range. The excitation source was a modulated 405 nm laser diode. An Olympus water immersion 60× (NA 1.2) objective lens was used with fluorescence emission being selected using a filter cube with an excitation 385–425 nm bandpass filter, 405 nm dichroic mirror, and 410 nm long pass emission filter. The fluorescence emission is then passed through a second filter cube with a 570 nm dichroic mirror and 510–560 nm (green) and 575–650 nm (red) emission filters. This second filter cube provides for simultaneous two channel measurements. In each channel, the emission was then directed through a pinhole (141 or 1000 μm diameter) and then onto the photomultiplier tube detector (Fig. 1). Samples were mounted on an XYZ piezo-controlled stage that allowed for both XY and XZ sections to be collected. For lifetime measurements, data was recorded using a minimum of 20 different frequencies, with the system being calibrated by measuring the absolute modulation ratio and phase of known, mono-exponential decaying, reference standards, HPTS (5.4 ns), RhB (1.74 ns), and eosin Y (1.07 ns). A detailed description of constructing FLIM images and energy transfer equations were described before [26,35] and can be also found in the Supplementary data. All the imaging analysis and fitting were done using the VISTA software provided with the Alba instrument.

The fluorescence decay data were fitted by a sum of exponentials ($\sum a_i e^{-t/\tau_i}$), to obtain the lifetime τ_i, average lifetimes, and pre-exponential values, a_i. The average fluorescence lifetime is calculated from the best-fit parameters using the equations:

$$\tau_{av} = \sum f_i \tau_i \quad (3)$$

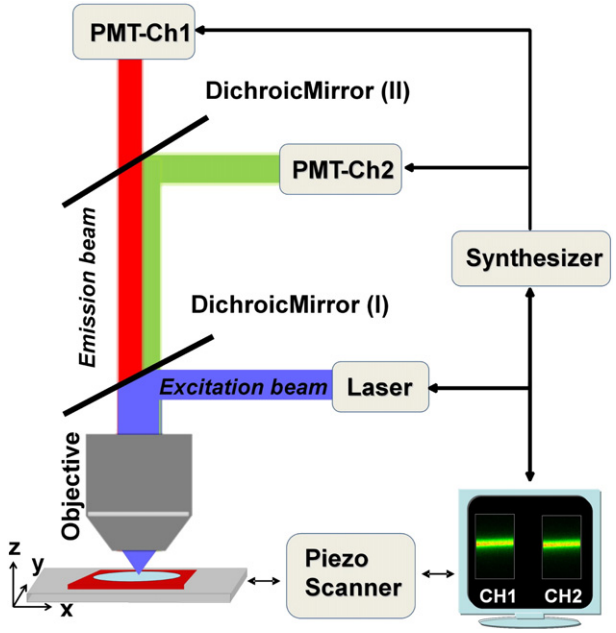

Fig. 1. Schematic outline of the two channel ISS Alba FLIM system used in this study. The excitation source is a 405 nm modulated laser diode.

$$f_i = a_i\tau_i / \sum a_i\tau_i \quad (4)$$

where f_i is the contribution factor of exponential term i^{th}, in all cases a bi-exponential fit was used. For FRET studies, the more appropriate lifetime expression is the amplitude-weighted fluorescence lifetime $<\tau>$ because it is proportional to the steady-state fluorescence intensity. $<\tau>$ is calculated by:

$$\langle\tau\rangle = \sum a_i \times \tau_i. \quad (5)$$

FRET efficiencies and D–A distances were calculated using well established equations (see Eqs. S5–7 Supplementary data). We note that these equations apply to distinct D–A distance. In our studies, where more than one pair is present in the hetero labeled protein, the distance obtained by the overall fluorescence decay measured with FLIM approach are treated as an overall average D–A distance.

3. Results and discussion

3.1. FRET in doubly labeled BSA

The choice of donor–acceptor (D–A) pair is critical for the application of FLIM–FRET studies and ideally, a Förster radius (R_0) that is approximately the same size as the protein being investigated is required. The native BSA structure in solution is usually regarded as having a prolate ellipsoid shape with approximate dimensions of 140 Å and 40 Å [36]. Therefore the Fluorescein–Tetramethylrhodamine donor–acceptor pair was selected as it had reported R_0 values in the 49–54 Å range [21]. When conjugated to BSA there is considerable spectral overlap as shown by the fluorescein emission spectrum of the BSA-F1 and the TMR absorption spectrum of the BSA-T1 (Supplementary data). Using the fluorescence quantum yield of donor $\varphi_D^0 = 0.71$ [37], an approximate R_0 value of 51 Å was estimated under our experimental settings.

Comparing the absorption spectra of BSA-F4-T2 with that of a mixture of approximately the same molar ratio of BSA-F1 and BSA-T1 shows some shift in the peak maxima of the absorption bands and some broadening in the double labeled protein (BSA-F4-T2) spectrum (Fig. 2a). This may indicate that the photophysical processes induced by the presence of two different fluorophores in the same protein molecule cause observable spectral changes [38,39]. The brightness of the doubly labeled construct could be improved by increasing fluorophore conjugation ratios. One advantage in increasing the number of dyes is to improve the sensitivity of tracking the structural changes of the labeled protein. However, due to the fact that the labeling reaction is not regioselective, the exact location of the probes on the protein structure is not certain. For example, the albumin structure contains 59 lysine aminoacids that can be conjugated with the isothiocyanate reactive groups of the fluorophores [36]. Another disadvantage of high fluorophore numbers is the increased possibility of self-quenching or energy migration between the donors which decreases the fluorescence quantum yield. Energy migration has been observed for fluorescein labeled human serum albumin [40] and, recently, in BSA labeled with more than three fluorescein molecules; a separation distance between fluorescein donor and acceptor, of approximately 53 Å was determined [38].

The steady-state optical properties of the doubly labeled BSA-F4-T2 construct used for the protein–surface measurements are summarized in Fig. 2. The fluorescence spectra is composed of the emission bands of fluorescein (F) and tetramethylrhodamine (TMR), with the TMR center being excited additionally via Energy Transfer from the F donor. For the unbound fluorophores, the fluorescence quantum yield of TMR is around one third of that for the fluorescein used to attach to amine or sulfhydryl aminoacid residues [37]. In addition, for BSA-F1 and BSA-T1, the molar absorptivity coefficients at the excitation wavelength for fluorescein and TMR are approximately the same (~3000 M^{-1} cm^{-1}).

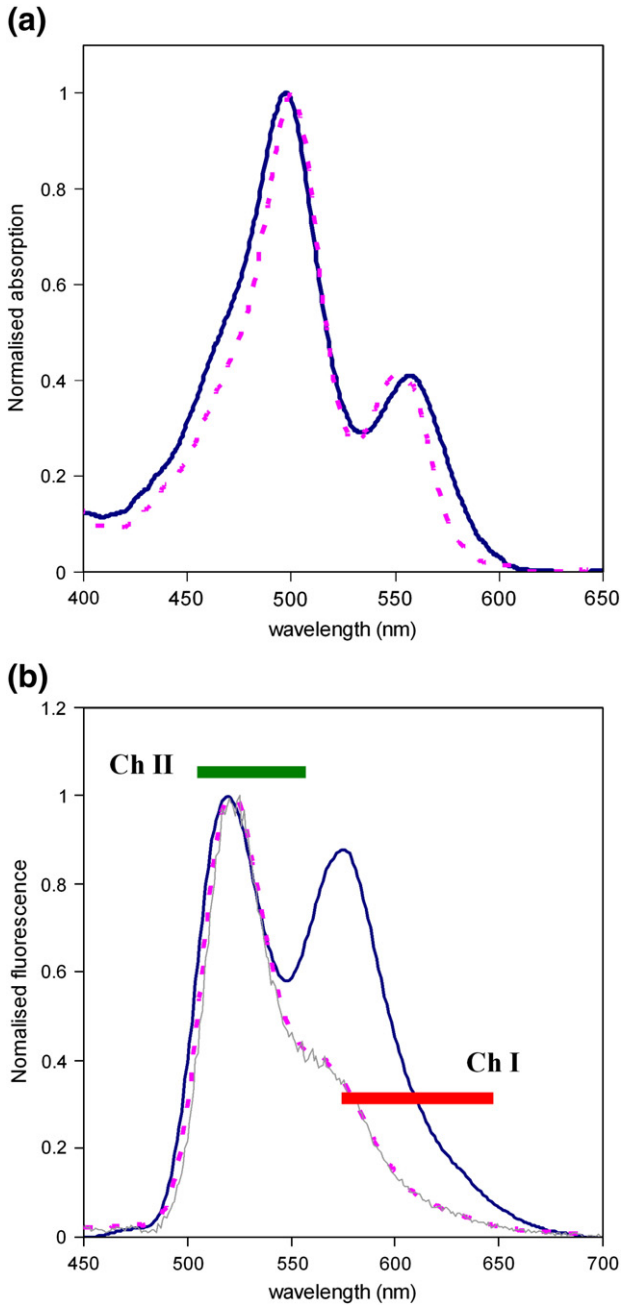

Fig. 2. (a) Electronic absorption spectra, and (b) fluorescence emission spectra obtained at 405 nm excitation for a solution of the doubly labeled BSA-F4-T2 (solid line), a solution comprising of a mixture (2:1 molar ratio) of BSA-F1 and BSA-T1 (dotted line), and simulated 4 × BSA-F1 + 2 × BSA-T1 (gray colored line). The fluorescence emission is split into two separate, green (fluorescein, Ch II) and red (T, Ch I) detector channels and the bars in (b) represent the full width half maxima of the band pass filter sets used for each channel.

If we assume no interaction between the two fluorophores (the control case), and also that the fluorescence quantum yields of the unbound fluorophores can be used in BSA-F1 and BSA-T1, respectively, then we can simulate the fluorescence emission spectrum by taking the emission spectra of the individually labeled species (BSA-F1 and BSA-T1) and combining them mathematically as represented by the thin grey line in Fig. 2b. This is in very good agreement with the experimentally measured spectra collected from a mixture (2:1 molar ratio) of the two singly labeled proteins represented by the dotted line in Fig. 2b. Comparing these control spectra to the emission of the BSA-F4-T2 construct, shows a clear increase in the intensity of the 576 nm

band which is caused by TMR center fluorescence via energy transfer from the F donor.

Energy transfer is also observed for BSA-F6-T1 with large changes in the red/green emission intensity ratio compared to the mathematically simulated spectrum. The BSA-F5 construct is the closest (in structure and photophysical behavior) fluorescein labeled protein without TMR which can be used to verify that FRET process is observed in BSA-F6-T1. Since the photophysical properties of the fluorescein labeled BSA is almost unchanged for proteins conjugated with more than three fluorescein molecules [38] we would expect only small differences in emission properties between BSA-F5 and BSA-F6. We observe that the fluorescence lifetimes of fluorescein molecules in BSA-F6-T1 are shorter than in BSA-F5 (Tables 1 and 2). Excitation spectra of the BSA-F6-T1 construct were obtained by monitoring emission at 670 nm (where TMR is the major contributor to the total fluorescence in BSA-T1), and the spectra shows excitation bands at 557 nm (expected TMR band) and an enhanced 499 nm (fluorescein band). Comparing this data to the excitation spectra of BSA-F5 and BSA-T1 under the same experimental conditions also indicates FRET (for more details see Fig. S4).

3.2. The fluorescence lifetime model

The fluorescence lifetime of fluorescently labeled proteins is quite complex because the fluorophore(s) can experience a variety of microenvironments. Usually, a multi-exponential model has to be used to completely explain the fluorescence decay process of protein bound fluorophores [27]. For example, we found that for BSA-F1 the fluorescence intensity decay was satisfactorily modeled by a bi-exponential fit which is in agreement with previously reported studies for BSA and other proteins [38]. A detailed assignment of the lifetime values and fractional intensities or amplitudes is not included because of the difficulty associated with assignment of a physical meaning to each individual exponential term in a multi-exponential model and can lead to misleading interpretations [27]. An alternative approach which could also be used is the recently developed model free analysis of the FLIM data that is based on the polar plot representation of frequency-domain data [41–43]. Here for simplicity we have used, the average fluorescence lifetimes (τ_{av}, Eq. (3)) calculated from a bi-exponential model (using multi-frequency measurements) for the general discussion, except when we discuss the FRET analysis. For FRET where the fluorophores have complex fluorescence decays, the τ_{av} values should not be used for calculating energy transfer efficiencies (and therefore D–A distance) because τ_{av} is not proportional to the steady-state intensity [21]. Thus the most appropriate average lifetime to use for FRET is the amplitude-weighted fluorescence lifetimes ($\langle\tau\rangle$, Eq. (5)). Tables 1 and 2 give the detailed lifetime data for $\langle\tau\rangle$ and τ_{av} values for all the constructs studied.

Table 1
Fluorescence decay parameters for the homo labeled BSA.

Construct	Medium	τ_1 (ns)	τ_2 (ns)	a_1	a_2	$\langle\tau\rangle$ (ns)	τ_{av} (ns)
BSA-F1	Bulk	0.81	3.91	0.38	0.62	2.73	3.56
(green channel)	Hydrophilic	0.81	3.68	0.65	0.35	1.81	2.85
	Hydrophobic	0.67	2.95	0.53	0.47	1.74	2.48
BSA-F5	Bulk	0.64	3.62	0.60	0.40	1.83	3.01
(green channel)	Hydrophilic	0.52	2.74	0.67	0.33	1.25	2.12
	Hydrophobic	0.60	2.23	0.67	0.33	1.14	1.65
BSA-T1	Bulk	1.22	3.40	0.48	0.52	2.35	2.86
(red channel)	Hydrophilic	0.87	2.68	0.53	0.47	1.72	2.20
	Hydrophobic	1.07	2.52	0.47	0.53	1.84	2.13
BSA-T7	Bulk	0.57	2.56	0.63	0.37	1.31	2.01
(red channel)	Hydrophilic	0.43	1.71	0.74	0.26	0.76	1.18
	Hydrophobic	0.43	1.01	0.65	0.35	0.63	0.75

Table 2
Fluorescence decay parameters for hetero labeled BSA constructs obtained from the green channel.

Construct	Medium	τ_1 (ns)	τ_2 (ns)	a_1	a_2	$\langle\tau\rangle$ (ns)	τ_{av} (ns)
BSA-F4-T2	Bulk	0.44	3.32	0.81	0.19	0.99	2.26
	Hydrophilic	0.64	3.18	0.82	0.18	1.10	1.97
	Hydrophobic	0.33	2.54	0.98	0.02	0.37	0.62
BSA-F6-T1	Bulk	0.50	3.22	0.78	0.22	1.10	2.25
	Hydrophilic	0.52	2.80	0.82	0.18	0.92	1.74
	Hydrophobic	0.64	1.91	0.73	0.27	0.98	1.30

The lifetime variations can be understood as arising from structural changes of the BSA host protein [26,27]. Therefore, changes in τ_{av} or $\langle\tau\rangle$ values can be related to surface-induced changes in the BSA structure as compared to the native BSA structure in bulk solution. The adsorption of the singly labeled proteins (BSA-F1, BSA-F5, BSA-T1, and BSA-T7) onto hydrophilic and hydrophobic surfaces was first studied using confocal FLIM sections to generate control data. To develop the initial experimental conditions, we used the BSA-F5 and BSA-T7 constructs because of their high brightness and better resistance to fading.

3.3. Single frequency FLIM

Using BSA-F5 in pH 7.4 buffered solutions which are left in contact with two different surfaces, the single frequency (100 MHz), XZ section (right angle section across the surface) fluorescence intensity and FLIM images (16×512 pixels) in Fig. 3 show significant differences in fluorescence. For the hydrophobic surface we observe a strong fluorescence signal on the surface due to the deposition of the protein, Fig. 3a, with a mean fluorescence lifetime of 1.7 (±1.9) ns, Fig. 3c. The mean fluorescence lifetime here is the value obtained resulting from the average of fluorescence lifetimes obtained for each

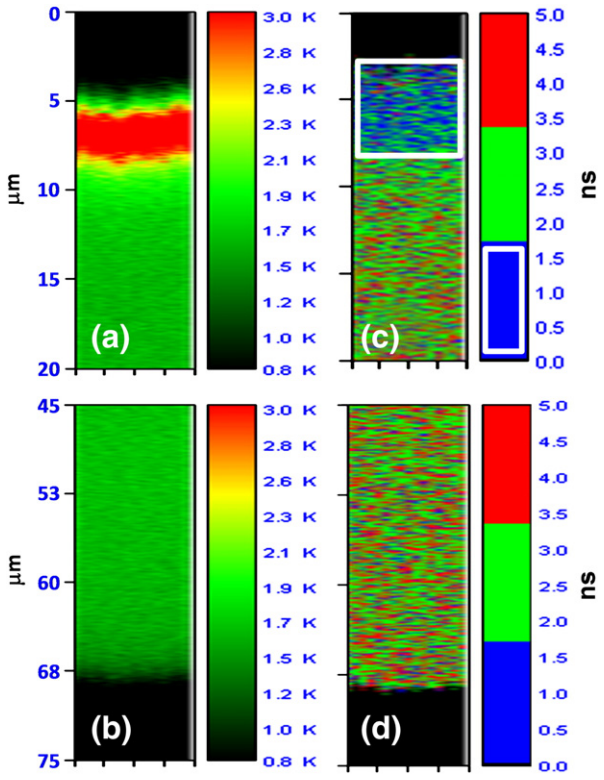

Fig. 3. Confocal fluorescence intensity images of BSA-F5 under PS+ experimental conditions for: (a) hydrophobic, (b) hydrophilic surfaces, and the respective FLIM images (c) and (d) obtained at 100 MHz. The white rectangle in (c) is included for clarity in the noncolor print to indicate the short lifetime region.

pixel in the image and so, no fitting is employed (see Eqs. S1 and S2). The hydrophilic surface in contrast, shows a uniform intensity, Fig. 3b, from bulk to surface and the mean fluorescence lifetime for the BSA-F5 is the same on the surface as it is in the bulk, 3.4 (±2.5) ns as observed for the XZ scanned section, Fig. 3d. The absence of the strong fluorescence signal on the hydrophilic surface may indicate that less protein is adsorbed on this surface compared to the hydrophobic surface (Fig. 3a). Although, the single frequency XZ FLIM imaging generates a rapid image with a relatively good contrast for qualitative assessment of the lifetime differences between the surface and bulk solution, the lifetime data is not accurate enough for FRET analysis and multi-frequency data is required [26].

3.4. Multi frequency FLIM

Using multi-frequency FLIM images, more accurate lifetimes for the BSA-F5 fluorescence in the green channel are obtained and these show differences between the bulk solution, hydrophilic and hydrophobic surfaces (Fig. 4). Fitting the averaged FLIM phase-modulation data to a bi-exponential model, we find that τ_{av} (for the PS+ case) is largest for the BSA-F5 in solution, 3.0 (±0.1) ns. On the glass surfaces, τ_{av} is lowest for BSA-F5 adsorbed on the hydrophobic surface, 2.1 (±0.2) ns, which is smaller than that observed for BSA-F5 adsorbed on a hydrophilic surface, 2.7 (±0.2) ns. The decay parameters obtained from the multi-frequency FLIM data (in the green and red channels) for all the different protein constructs are listed in Tables 1 and 2.

3.5. PS+ versus PS−

Removal of the bulk labeled BSA solution from above the surface (the PS− case), results in a general decrease in the decay times of the deposited protein films (Supplementary data). This shows that the presence of the bulk solution contaminates the signal from the adsorbed layer. Perhaps, because the conventional confocal microscope only provides a z-axis resolution of ~2 μm (under our experimental conditions) at best, it is not sufficient to avoid collecting out-of-focus emission in the PS+ cases. Increasing the confocal resolution requires the use of smaller pinhole apertures, but this also reduces the fluorescence signal very significantly, making FLIM measurements less accurate. In some cases (PS− for hydrophilic surfaces) the fluorescence signal was too weak for FLIM measurements under normal confocal conditions and so the system had to be operated in an almost non-confocal mode to increase light throughput. For real-world applications where we do not want to disturb the biological system in contact with the surface, we would like to operate in the PS+ mode. Furthermore this mode would enable real-time measurements thus enabling the observation of the primary adsorption processes. However, when we compare the two protocols, the PS− protocol shows larger fluorescence lifetime differences between the surfaces, because the bulk solution contamination is removed. Thus, for conventional confocal microscopy removing bulk solution after the incubation is more appropriate for our experiments.

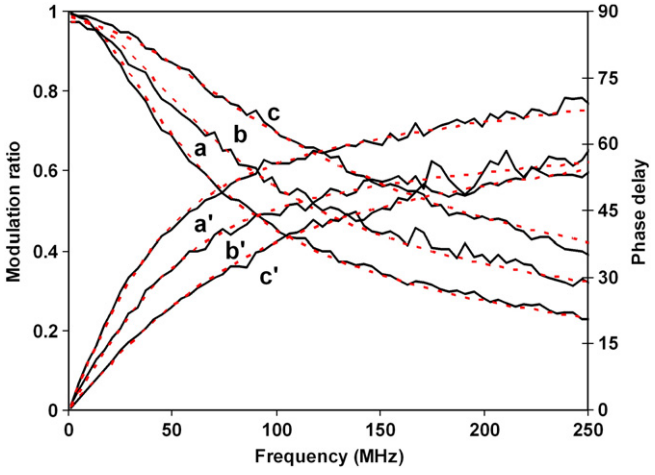

Fig. 4. Average modulation ratios (a, b, c) and phase delays (a', b', c') for BSA-F5 (PS+ conditions) measured in bulk (a, a'), on a hydrophilic surface (b, b'), and on a hydrophobic surface (c, c'). The dashed lines represent the best bi-exponential fitting curves. The data was extracted from the 32×32 pixel multi-frequency FLIM images.

3.6. Adsorption of singly labeled BSA

The fluorescence lifetimes obtained from green and red channels, respectively, of BSA-F1 and BSA-T1, are highest in the bulk solution, and lowest on surfaces (Tables 1 and 2, and Fig. 5). Since there is one probe per protein, the decrease of average fluorescence lifetime in BSA-F1 and BSA-T1 on surface adsorption must be caused by other factors such as refractive index (RI) and fluorescence quenching [44,45]. The RI effect on the lifetime of the labeled proteins was studied by measuring lifetimes in water–glycerol mixtures (1.33–1.46)[45]. Changes in RI in the fluorescent probe environment can be expected when the protein is deposited on solid surfaces [46]. For BSA-F1, the RI effect accounts for a reduction of τ_{av} of around 11% that is, only one third of the reduction of τ_{av} observed when BSA-F1 is deposited on hydrophobic surfaces (Supplementary data). For the BSA-T1 construct, the opposite effect was observed and the τ_{av} in water–glycerol mixtures increased by up to 21%. The difference in lifetime trends between the two constructs may be explained by differences in the radiative and non-radiative rate constant ratios for

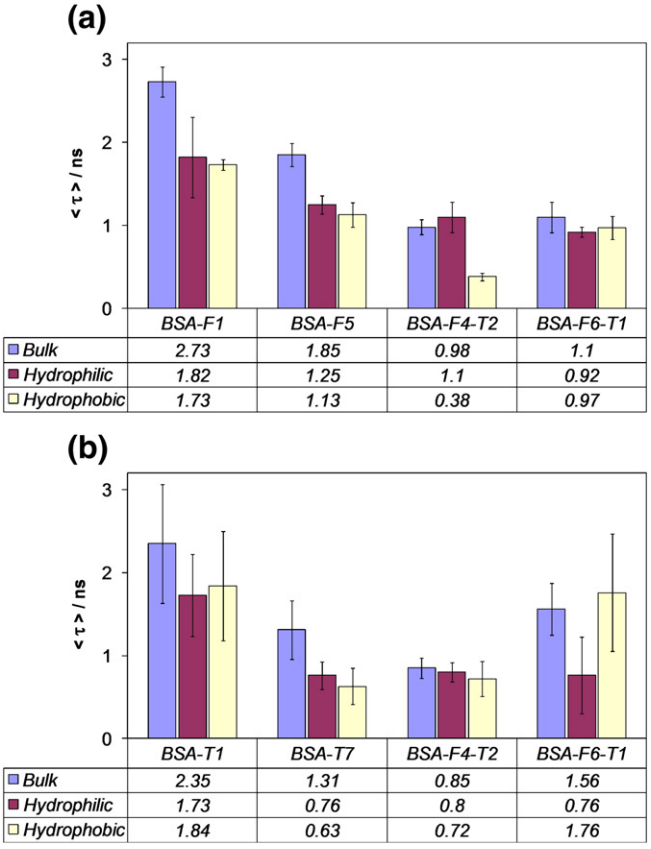

Fig. 5. Amplitude-weighted average fluorescence lifetimes of the various labeled proteins in solution and on different surfaces as measured in the green (a) and red (b) channels.

the two fluorophores. For fluorescein, the radiative rate constant is approximately one order of magnitude greater than the non-radiative rate constant [47], whereas for rhodamine, rate constants are of the same order of magnitude [48,49]. In the water–glycerol mixtures, we have also to consider viscosity effects, which are important in compounds where the non-radiative rate constant is of same order or larger than the radiative rate constant. Therefore, for BSA-T1, the viscosity induced increase in τ_{av} will outweigh the decrease in τ_{av} generated by the RI effect on the radiative rate constant. For BSA-F1, the opposite is true and the RI effect outweighs the viscosity effect leading to a decrease in τ_{av}. These results show that the RI effect does not fully account for the surface adsorption induced changes in τ_{av}. Another factor to consider is that fluorescence quenching of xanthene based fluorophores, such as fluorescein and rhodamine, by the amino acids tryptophan (Trp) and tyrosine (Tyr) can also cause decreases in lifetime [50]. The efficiency of the process is based on the distance between Trp/Tyr and fluorescein [19] and this is very sensitive to structural conformation. BSA has 20 Tyr, and two Trp residues [36], and thus one expects that the fluorescence emission properties of fluorescein, tetramethylrhodamine, or both, will be affected.

3.7. Adsorption of homo labeled BSA

For BSA-F5 and BSA-T7, τ_{av} and $\langle\tau\rangle$ are lower compared to BSA-F1 and BSA-T1 (Fig. 5) which may be due to self-quenching or energy migration [38,40]. However, another possibility is that the extra conjugated fluorophores can be located on sites in close proximity to aminoacids (Tyr or Trp), which could quench the fluorescence. In this case, the contribution of those extra fluorophores in the total fluorescence decay would result in a decrease in lifetimes. Irrespective of which factors are responsible for the reduction of fluorescence lifetimes of BSA-F5 and BSA-T7 (when compared to BSA-F1 and BSA-T1, respectively), the possibilities discussed above are distance dependent effects. Therefore, when there are structural changes in the highly labeled proteins, one will expect that there will be related changes in the fluorescence emission.

Although BSA-F5 and BSA-T7 show a decrease in the decay times when deposited on solid surfaces when compared to the bulk media, both show small lifetime differences (but larger than those observed for BSA-F1 and BSA-T1) when they are adsorbed on different surfaces (Fig. 5). That is, the lifetimes obtained in the green channel are slightly higher for BSA-F5 on the hydrophilic surface compared to the hydrophobic surface. The same trend can be observed for BSA-T7 red channel lifetimes. They are brighter than their homologues (BSA-F1 and BSA-T1) however, the lifetimes differences are not sufficient to differentiate between the different surfaces.

3.8. Adsorption of hetero labeled BSA

The detection of fluorescence signal in the green channel must be analyzed with care due to the possibility of detection of red fluorescence, e.g. cross-talk. In our experimental setup, we were not able to eliminate completely the fluorescence signal from the TMR at short edge tail of the fluorescence band up to 560 nm. To properly exclude TMR fluorescence, a bandpass filter with an upper limit of 530 nm should be used. Although, the estimated amount of TMR emission can be small for BSA-F4-T2 in bulk solution, this cross-talk increases with the increase of energy transfer efficiency. From our data we observe that the greatest energy transfer efficiency is obtained for BSA-F4-T2 adsorbed onto the hydrophobic surface. We note that the $\langle\tau\rangle$ obtained for BSA-T1 on a hydrophobic surface in the red channel (1.84 ns) is larger than the value obtained for BSA-F4-T2 adsorbed on a hydrophobic surface in the green (0.37 ns). Thus if there is contamination the true $\langle\tau\rangle$ for BSA-F4-T2 adsorbed on a hydrophobic surface should be smaller than 0.37 ns. This means that the energy transfer value obtained for BSA-F4-T2 adsorbed on the hydrophobic surface has to be considered as the lower limit, i.e., the ET efficiency is even higher than that determined. In the case of BSA-F6-T1, where the apparent energy transfer efficiency for adsorption on a hydrophobic surface is smaller than that observed in the bulk, the fluorescence cross-talk in the green channel will be relatively small compared to the BSA-F4-T2 case.

For the green channel, if we take the bulk solution as a reference, we note that $\langle\tau\rangle$ for the hetero constructs follow different trends when they are adsorbed on surfaces (Fig. 5a). For BSA-F4-T2, $\langle\tau\rangle$ is slightly longer on the hydrophilic surface compared to the bulk solution, whereas for BSA-F6-T1 the opposite is true for the same surface. Conversely for hydrophobic surfaces, BSA-F4-T2 shows the larger decrease in lifetimes compared to the BSA-F6-T1 construct. Perhaps this difference is because of the presence of two TMR acceptors that enhances energy transfer, and thus is more sensitive to structural changes (*vide infra*). These results suggest that the BSA-F4-T2 construct is a good candidate molecule for studying these surface-induced effects.

The analyses of the red channel lifetime data for the hetero conjugated protein cannot be made, because the mixture of energy transfer excited TMR acceptors with those directly excited by the 405 nm excitation source can complicate the interpretation of the red fluorescence intensity decays. In addition, we must also consider that some fluorescein emission will contribute to the total emission detected in the red channel, as illustrated in Fig. 2b. This fluorescein contribution can be enhanced when there is an increase of red emission quenching or when we use a construct with a high F/T molar ratio. The fluorescence quenching of rhodamine by amino acid residues is much less efficient than that for fluorescein [50]. However, it has been reported, that decreases of fluorescence intensity and lifetime of TMR were observed when a fluorescein based molecule was bound to a nucleic acid structure with at least 24 base pairs of separation [51]. In this case, the possibility of TMR being quenched by fluorescein cannot be ruled out. Moreover, the red channel fluorescence signal from the hydrophilic surfaces was very weak which would increase the probability of detecting a significant contribution from the fluorescein emission. For BSA-F4-T2, the analysis of red channel data has an extra complication because of the possibility for the two TMR to be labeled in a site relatively close to each other, which could allow an exciton coupling [52,53]. Thus the emission properties would depend strongly on the closeness and orientation of the two Ts. Therefore, we cannot provide an unambiguous analysis of the $\langle\tau\rangle$ values obtained in the red channel for BSA-F4-T2.

3.9. Average donor–acceptor distance of deposited proteins

The observed protein structural changes are caused by a variety of factors that depend on physicochemical properties of the protein, the surface, and the aqueous environment. The hydrophobic (or hydrophilic) character of a surface is usually expressed by its wettability, which is typically measured by the contact angle that a drop of water makes on the surface [9,31] or recently by fluorescence probes [54]. In aqueous solutions, the polar residues of BSA are, in general, more exposed to the bulk solution than nonpolar groups. When BSA comes into contact with a hydrophobic surface, a structural rearrangement occurs which can be observed by FRET. This happens because in the native conformation the hydrophobic pockets of the protein which are internally located need to be exposed to the hydrophobic surface to promote adsorption [9,10]. The interaction of BSA with hydrophilic surfaces can be either attractive or repulsive depending on the net driving force of the system. At pH 7.4, both the hydrophilic surface and BSA are negatively charged, thus mutually repulsive which helps explain why less protein is deposited on the hydrophilic surface. However, some BSA does adsorb on this surface due to dispersion forces which can lead to some structural changes [18]. It is, therefore, the balance between electrostatic and dispersion forces (as

determined by enthalpic contribution) that plays an important role in structuring the protein in the deposited layer on the surfaces. In the analysis of the fluorescence approach used to determine how the protein structure is affected by the surface chemistry, a clear dependence on where the donor and acceptor probes are located in BSA and the FRET efficiencies are expected.

As we have already mentioned, the spectral properties and fluorescence lifetimes are very similar when the BSA-fluorescein conjugation generates a ratio greater than three fluorophores per protein, i.e., BSA-F4, BSA-F5, and BSA-F6. Using the green channel $\langle\tau\rangle$ data obtained for BSA-F5, the energy transfer (ET) efficiency and, therefore, the average distance between fluorescein and TMR can be calculated (using Eqs. S5–7, Supplementary data) and the results are displayed in Tables 3 and 4.

We note small differences in the ET efficiency values between both hetero constructs (BSA-F4-T2 and BSA-F6-T1), when they are in the bulk. In the deposited layer on hydrophilic surfaces, where the detected signals were low, the FRET efficiency observed for BSA-F6-T1 is ca. two-fold of that for BSA-F4-T2. In the case of BSA-F4-T2 where the fluorescein emission intensity is expected to be smaller than that for BSA-F6-T1, the contribution of the red fluorescence in the green channel will increase with the increase of excitation energy. Moreover, fluorescein photobleaching would further enhance the contribution of TMR emission in the green channel, reducing the FRET efficiency obtained for BSA-F4-T2. Despite the differences in the two constructs, the ET efficiency decreases when they are adsorbed on hydrophilic surfaces. This decrease may be explained by an increase of the average distances between the fluorescein and TMR centers. The major distinction between these hetero constructs in the ET efficiency is observed when they are adsorbed on more hydrophobic surfaces, for BSA-F6-T1 it is 14% while for BSA-F4-T2, it is but 67%. This opposite trend between both constructs when adsorbed on the same surface shows the importance of having more than one TMR in the doubly labeled protein.

The BSA-F4-T2 construct shows the largest changes because of the presence of a second TMR acceptor, which is probably attached to a region that is structurally most affected by the adsorption process, causing a reduction in the average D–A distance. In this case, the average distance between fluorescein and T centers in BSA-F4-T2 decreases on going from the bulk solution to the hydrophobic surface and increases for the hydrophilic surface. The observations may indicate that some part of the protein structure stretches slightly when it is adsorbed on a hydrophilic surface (as observed for BSA-F6-T1) and contracts when on the hydrophobic surface. In the case of the contraction we would suggest that this may occur in the region of the protein where the second TMR in BSA-F4-T2 is most likely located, while the expansion may happen in the region where TMR is located in BSA-F6-T1. Assuming that the protein structure is extended on the hydrophilic surface, less space would be available for the adsorption of further proteins. Whereas, if the protein structure is partially contracted (or compacted), more protein can fit on the surface. This would mean that more protein can be adsorbed on the hydrophobic than hydrophilic surfaces, which has been observed using other techniques [9,11].

The BSA concentration on these hydrophilic surfaces is around 0.9 mg/m^2 [18] while on a hydrophobic surface (polystyrene) it is ~2.3 mg/m^2 [9]. Using the BSA-F4-T2 molecular weight (~68.4 kDa), the surface area occupied by an adsorbed protein can be estimated. Each BSA-F4-T2 molecule will occupy an area of 1.26×10^4 Å^2 on a hydrophilic surface, and 0.49×10^4 Å^2 on a hydrophobic surface. This is approximately a square of side 112 Å and 70 Å, respectively. Since the BSA structure can be roughly considered as a prolate ellipsoid shape with dimensions of 140 Å and 40 Å [36], one can expect that the major BSA conformation to adsorb on a hydrophilic surface is "side-on" while in the hydrophobic is "end-on". In the side-on conformation, the long axis lies parallel to the surface, while in the end-on conformation the short axis is parallel to the surface. Thus the probability of intermolecular FRET between adsorbed proteins will be higher on hydrophobic surfaces than on hydrophilic surfaces. From our data, only BSA-F4-T2 on a hydrophobic surface showed very significant energy transfer which also could be partly due to intermolecular FRET. This means that the average distance between the FRET pairs can be directly related to the density of the deposited layer.

We acknowledge that the unknown probe locations are a major drawback which prevents a more accurate determination of how the protein structure and orientation are affected by the surface interactions. However, the use of these doubly labeled constructs clearly shows variations in energy transfer efficiencies on different surfaces. Since this is related to changes in the average distances of the donor and acceptor fluorophores, the data can be used to monitor surface-induced structural changes of the deposited protein layer. For this end, the BSA-F4-T2 construct was shown to be the more appropriate probe for observing surface-induced changes.

Table 3
Energy transfer efficiency (%) between donor–acceptor centers in the hetero doubly labeled protein constructs in solution and on surfaces, using BSA-F5 as a donor, respectively, for each medium.

Medium	E (BSA-F4-T2)	E (BSA-F6-T1)
Bulk	46 ± 6	40 ± 8
Hydrophilic	12 ± 2	26 ± 3
Hydrophobic	67 ± 12	14 ± 3

Table 4
Average donor–acceptor distance (in R_0 units) of the hetero doubly labeled protein constructs in solution and on surfaces, using BSA-F5 as a donor, respectively, for each medium.

Medium	R (BSA-F4-T2)	R (BSA-F6-T1)
Bulk	1.03 ± 0.04	1.07 ± 0.06
Hydrophilic	1.39 ± 0.05	1.19 ± 0.03
Hydrophobic	0.89 ± 0.08	1.36 ± 0.05

4. Conclusions

This confocal, FLIM–FRET method using these Fluorescein-BSA-T constructs may be used to probe the different microenvironments that serum proteins experience on surfaces. In this work, we have explored several parameters that are relevant for this approach to be used as a tool in the determination of protein structural changes induced by the surfaces during adsorption. Some issues must be considered in measuring the fluorescence lifetimes of the labeled protein adsorbed on hydrophilic surfaces, because of low signal levels (perhaps due to low amounts of protein deposited), the lack of optical resolution to discriminate emissions between the deposited protein and the bulk solution above the surface containing the fluorescently labeled protein. When the protocol is modified to remove the bulk protein solution after incubation, we were able to obtain more reliable results.

The influence of effects such as refractive index, viscosity and aminoacid residue quenching must also be considered in this FLIM–FRET method. Fortunately, these effects can be reduced or eliminated by always using the singly labeled proteins (with only donors) as controls (in solution and on surfaces). Thus surface effects can be resolved using FLIM–FRET via a detailed comparison of the fluorescence intensity and lifetime data from the hetero labeled protein constructs with the data from the singly labeled BSA constructs. The BSA-F5, BSA-T7, and BSA-F6-T1 constructs were found to be very bright and thus making them very good for discriminating between the bulk and surface regions in FLIM images, either by intensity or by fluorescence lifetime. However, they were shown to be unable to distinguish between the glass surfaces i.e. surface hydrophilic or hydrophobic character. Using the experimental setup described, we

were unable to completely eliminate cross-talk of red fluorescence into green channel. Thus the small contribution from the TMR fluorescence will affect the fluorescence decays detected by the green channel. Although, this would not be a major problem for the BSA-F6-T1 construct, the results for BSA-F4-T2 on hydrophilic surfaces must be interpreted and analyzed with care to account for cross-talk because of the low fluorescence signal detected in the green channel, and the expected reduction of fluorescein fluorescence by FRET. We have found that the BSA-F4-T2 construct was the best fluorescent model protein to probe the differences of the surfaces, in the way that they induce the structural changes of the adsorbed protein. Using BSA-F5 as the only donor in the FRET pair, the interaction of BSA-F4-T2 with surfaces of different polarities show two distinct effects when compared to the protein structure present in the bulk solution; that is, the average FRET pair distance increases when the protein adsorbs onto a hydrophilic surface, while on a hydrophobic surface that average distance decreases. The F–T FRET pair is not the best probe, because of the lack of labeling control (position and number), some photobleaching, and a relatively small range of lifetime changes. Despite these limitations, these FLIM–FRET results show that the protein structure can be affected differently by the nature of the surface upon which it is deposited. In the future, the use of brighter and more specific fluorescence labels should increase the potential of this FLIM–FRET method for the rapid characterization of surface-induced structural changes in proteins (and possibly surface orientation), and thus better designed adaptive biomaterials for medical applications.

Acknowledgments

We thank Noemie Marguerite for the protein bioconjugation. This work was supported by funding from the National Biophotonics Imaging Platform, an Irish Higher Education Authority Programme for Research in Third Level Institutions, and a Science Foundation Ireland Principal Investigator Grant (number 02/IN.1/M231 and 02/IN.1/M231S1 to AGR).

Appendix A. Supplementary data

Supplementary data associated with this article can be found, in the online version, at doi:10.1016/j.bpc.2010.07.006.

References

[1] D.G. Castner, B.D. Ratner, Biomedical surface science: foundations to frontiers, Surf. Sci. 500 (2002) 28–60.
[2] J.M. Anderson, Biological responses to materials, Ann. Rev. Mater. Res. 31 (2001) 81–110.
[3] W.J. Hu, J.W. Eaton, T.P. Ugarova, L. Tang, Molecular basis of biomaterial-mediated foreign body reactions, Blood 98 (2001) 1231–1238.
[4] E.J. Topol, P.W. Serruys, Frontiers in interventional cardiology, Circulation 98 (17) (1998) 1802–1820.
[5] R.A. Hermann, G. Schmidmaier, B. Markl, A. Resch, I. Hahnel, A. Stemberger, E. Alt, Antithrombotic coating of stents using a biodegradable drug delivery technology, Thromb. Haemost. 82 (1999) 51–57.
[6] A.M. Lincoff, E.J. Topol, S.G. Ellis, Local drug delivery for the prevention of restenosis: fact, fancy, and future, Circulation 90 (4) (1994) 2070–2084.
[7] E. Tziampazis, J. Kohn, P.V. Moghe, PEG-variant biomaterials as selectively adhesive protein templates: model surfaces for controlled cell adhesion and migration, Biomaterials 21 (2000) 511–520.
[8] J.J. Gray, The interaction of proteins with solid surfaces, Curr. Opin. Struc. Biol. 14 (2004) 110–115.
[9] K. Nakanishi, T. Sakiyama, K. Imamura, On the adsorption of proteins on solid surfaces, a common but very complicated phenomenon, J. Biosci. Bioeng. 91 (3) (2001) 233–244.
[10] H. Chen, L. Yuan, W. Song, Z. Wu, D. Li, Biocompatible polymer materials: role of protein–surface interactions, Prog. Polym. Sci. 33 (2008) 1059–1087.
[11] J. Benesch, A. Askendal, P. Tengvall, Quantification of adsorbed human serum albumin at solid interfaces: a comparison between radioimmunoassay (RIA) and simple null ellipsometry, Colloid Surf. B-Biointerfaces 18 (2000) 71–81.
[12] H. Elwing, Protein absorption and ellipsometry in biomaterial research, Biomaterials 19 (4–5) (1998) 397–406.
[13] J.R. Lu, X. Zhao, M. Yaseen, Protein adsorption studied by neutron reflection, Curr. Opin. Coll. Interf. Sci. 12 (2007) 9–16.
[14] C. Czeslik, Factors ruling protein adsorption, Z. Phys. Chem. 218 (7) (2004) 771–801.
[15] E. Ostuni, R.G. Chapman, R.E. Holmlin, S. Takayama, G.M. Whitesides, A survey of structure–property relationships of surfaces that resist the adsorption of protein, Langmuir 17 (18) (2001) 5605–5620.
[16] M.L. Gee, L. Lensun, T.A. Smith, C.A. Scholes, Time-resolved evanescent wave-induced fluorescence anisotropy for the determination of molecular conformational changes of proteins at an interface, Eur. Biophys. J. 33 (2004) 130–139.
[17] W. Norde, My voyage of discovery to proteins in flatland... and beyond, Colloid Surf. B-Biointerfaces 61 (2008) 1–9.
[18] D.M. Togashi, A.G. Ryder, G. Heiss, Quantifying adsorbed protein on surfaces using confocal fluorescence microscopy, Colloid Surf. B-Biointerfaces 72 (2009) 219–229.
[19] D.M. Togashi, A.G. Ryder, B. Szczupak, A. Calvet, M. O'Loughlin, Investigating tryptophan quenching of fluorescein fluorescence under protolytic equilibrium, J. Phys. Chem. A 113 (12) (2009) 2757–2767.
[20] H. Szmacinski, J.R. Lakowicz, Lifetime-based sensing, in: J.R. Lakowicz (Ed.), Topics in Fluorescence Spectroscopy: Vol. 4. Probe Design and Chemical Sensing, Plenum Press, New York, 1994, Chap. 10.
[21] J.R. Lakowicz, Principles of Fluorescence Spectroscopy, 3rd edSpringer, Singapore, 2006.
[22] S. Pelet, M.J. Previte, D. Kim, K.H. Kim, T.T. Su, P.T. So, Frequency domain lifetime and spectral imaging microscopy, Microsc. Res. Tech. 69 (2006) 861–874.
[23] F. Festy, S.M. Ameer-Beg, T. Ng, K. Suhling, Imaging proteins in vivo using fluorescence lifetime microscopy, Mol. BioSyst. 3 (2007) 381–391.
[24] D.M. Togashi, S.M.B. Costa, A.J.F.N. Sobral, Lipophilic porphyrin microparticles induced by AOT reversed microemulsions—a fluorescence lifetime imaging study, Biophys. Chem. 119 (2) (2006) 121–126.
[25] D.M. Togashi, R.I.S. Romão, A.M. Goncalves da Silva, S.M.B. Costa, A.J.F.N. Sobral, Self-organization of a sulfoamido-porphyrin in langmuir monolayers and langmuir-blodgett films, Phys. Chem. Chem. Phys. 7 (2005) 3874–3883.
[26] D.M. Togashi, A.G. Ryder, Fluorescence lifetime imaging study of a thin protein layer on solid surfaces, Exp. Mol. Pathol. 82 (2) (2007) 135–141.
[27] D.M. Togashi, A.G. Ryder, Time-resolved fluorescence studies on bovine serum albumin denaturation process, J. Fluoresc. 16 (2006) 153–160.
[28] A. Periasamy, Fluorescence resonance energy transfer microscopy: a mini review, J. Biomed. Opt. 6 (3) (2001) 287–291.
[29] E.A. Jares-Erijman, T.M. Jovin, Imaging molecular interactions in living cells by FRET microscopy, Curr. Opin. Chem. Biol. 10 (2006) 409–416.
[30] F.E. Bartell, H.H. Zuidema, Wetting characteristics of solids of low surface tension such as talc, waxes and resins, J. Am. Chem. Soc. 58 (1936) 1449–1454.
[31] T. Greg, Bioconjugation Techniques, 1st editionHermanso Academic Press, 1996.
[32] Invitrogen Molecular Probes Product information (It is assumed that ε_{494} value quoted for pH 8.0 is approximately the same as pH 7.4): http://probes.invitrogen.com/media/pis/mp06434.pdf.
[33] M. Cardamone, N.K. Puri, Spectrofluorimetric assessment of the surface hydrophobicity of proteins, Biochem. J. 282 (1992) 589–593.
[34] Invitrogen Molecular Probes Product information: http://probes.invitrogen.com/media/pis/mp06163.pdf.
[35] D.M. Togashi, A.G. Ryder, A fluorescence analysis of ANS bound to bovine serum albumin: binding properties revisited by using energy transfer, J. Fluoresc. 18 (2) (2008) 519–526.
[36] T. Peters Jr., All About Albumin: Biochemistry, Genetics, and Medical Applications, Academic Press, San Diego, CA, 1996.
[37] R.Y. Tiesen, L. Ernst, A. Waggoner, Fluorophores for confocal microscopy: photophysics and photochemistry, in: J.B. Pawley (Ed.), Handbook of Biological Confocal Microscopy, 3rd ed., Plenum Press, New York, 2006, pp. 338–352.
[38] G. Hungerford, J. Benesch, J.F. Mano, R.L. Reis, Effect of the labelling ratio on the photophysics of fluorescein isothiocyanate (FITC) conjugated to bovine serum albumin, Photochem. Phobiol. Sci. 6 (2007) 152–158.
[39] J. Hernando, M. van der Schaaf, E.M.H.P. van Dijk, M. Sauer, M.F. Garcia-Paraj, N.F. van Hulst, Excitonic behavior of rhodamine dimers: a single-molecule study, J. Phys. Chem. A 107 (2003) 43–52.
[40] J.R. Lakowicz, J. Malicka, S. D'Auria, I. Gryczynski, Release of the self-quenching of fluorescence near silver metallic surfaces, Anal. Biochem. 320 (2003) 13–20.
[41] M.A. Digman, V.R. Caiolfa, M. Zamai, E. Gratton, The phasor approach to fluorescence lifetime imaging analysis, Biophys. J. 94 (2) (2008) L14–L16.
[42] G.I. Redford, R.M. Glegg, Polar plot representation for frequency-domain analysis of fluorescence lifetimes, J. Fluoresc. 15 (5) (2005) 805–815.
[43] D.M. Jameson, E. Gratton, R.D. Hall, The measurement and analysis of heterogeneous emissions by multifrequency phase and modulation fluorometry, Appl. Spectrosc. Rev. 20 (1984) 55–106.
[44] C. Jones, K. Suhling, Refractive index sensing using Fluorescence Lifetime Imaging (FLIM), Second International Conference on Optical and Laser Diagnostics, 45 (223), 2006, doi:10.1088/1742-6596/45/1/031.
[45] J.W. Borst, M.A. Hink, A. van Hoek, A.J.W.G. Visser, Effects of refractive index and viscosity on fluorescence and anisotropy decays of enhanced cyan and yellow fluorescent proteins, J. Fluoresc. 15 (2) (2005) 153–160.
[46] J. Vörös, The density and refractive index of adsorbing protein layers, Biophys. J. 87 (2004) 553–561.
[47] M. Arık, N. Çelebi, Y. Onganer, Fluorescence quenching of fluorescein with molecular oxygen in solution, J. Photochem. Photobiol. A: Chemistry 170 (2005) 105–111.
[48] R.S. Moog, M.D. Ediger, S.G. Boxer, M.D. Fayer, Viscosity dependence of the rotational reorientation of rhodamine B in mono- and polyalcohols. Picosecond transient grating experiments, J. Phys. Chem. 86 (24) (1982) 4694–4700.
[49] J.A.B. Ferreira, S.M.B. Costa, L.F.V. Ferreira, Activated radiationless decay of rhodamine 3B: polarity and friction effects, J. Phys. Chem. A 104 (51) (2000) 11909–11917.

[50] N. Marmé, J.-P. Knemeyer, M. Sauer, J. Wolfrum, Inter- and intramolecular fluorescence quenching of organic dyes by tryptophan, Bioconjug. Chem. 14 (2003) 1133–1139.
[51] H. Kojima, N. Spataru, Y. Kawata, S.-I. Yano, I. Vartires, Long-range electron transfer Interaction between carboxyTMR and fluoresceinisothiocyanate bound covalently to DNA, as evidence by fluorescence quenching, J. Phys. Chem. B 102 (1998) 9981–9984.
[52] F. del Monte, D. Levy, Formation of fluorescent rhodamine B J-dimers in sol–gel induced by the adsorption geometry on the silica surface, J. Phys. Chem. B 102 (1998) 8036–8041.
[53] D.M. Togashi, S.M.B. Costa, A.J.F.N. Sobral, A.M. d'A.R. Gonsalves, Self-aggregation process of lipophilic porphyrins in reversed micelles of aerosol OT — (AOT), J. Phys. Chem. B 108 (2004) 11344–11356.
[54] B. Szczupak, A.G. Ryder, D.M. Togashi, A.S. Klymchenko, Y.A. Rochev, A. Gorelov, T.J. Glynn, Polarity assessment of thermoresponsive poly(NIPAM-co-NtBA) copolymer films using fluorescence methods, J. Fluoresc. 20 (3) (2010) 719–731.